Journal of Materials Chemistry B

RSC Publishing

PAPER

View Article Online
View Journal | View Issue

Self-assembly of amphiphilic peptides into bio-functionalized nanotubes: a novel hydrolase model

Cite this: *J. Mater. Chem. B*, 2013, **1**, 2297

Zupeng Huang, Shuwen Guan, Yongguo Wang, Guannan Shi, Lina Cao, Yuzhou Gao, Zeyuan Dong, Jiayun Xu, Quan Luo* and Junqiu Liu*

Herein, we report the construction of a novel hydrolase model *via* self-assembly of a synthetic amphiphilic short peptide (Fmoc-FFH-$CONH_2$) into nanotubes. The peptide-based self-assembled nanotubes (PepNTs-His) with imidazolyl groups as the catalytic centers exhibit high catalytic activity for *p*-nitrophenyl acetate (PNPA) hydrolysis. By replacement of the histidine of Fmoc-FFH-$CONH_2$ with arginine to produce a structurally similar peptide Fmoc-FFR-$CONH_2$, guanidyl groups can be presented in the nanotubes through the co-assembly of these two molecules to stabilize the transition state of the hydrolytic reaction. Therefore significantly improved catalytic activity has been achieved by the reasonable distribution of three dominating catalytic factors: catalytic center, binding site and transition state stabilization to the co-assembled peptide nanotubes (PepNTs-His-Arg_{max}). The resulting hydrolase model shows typical saturation kinetics behaviour to that of natural enzymes and the catalytic efficiency of a single catalytic center is 519-fold higher than that without catalysts. As for a nanotube with multi-catalytic centers, a remarkable catalytic efficiency could be achieved with the increase of building blocks. This model suggests that the well ordered and dynamic supramolecular structure is an attractive platform to develop new artificial enzymes to enhance the catalytic activity. Besides, this novel peptide-based material has excellent biocompatibility with human cells and is expected to be applied to organisms as a substitute for natural hydrolases.

Received 1st February 2013
Accepted 5th March 2013

DOI: 10.1039/c3tb20156b

www.rsc.org/MaterialsB

Downloaded by University of Tennessee at Knoxville on 18/04/2013 18:10:06.
Published on 05 March 2013 on http://pubs.rsc.org | doi:10.1039/C3TB20156B

Introduction

Natural enzymes are a type of highly efficient biocatalyst. Compared to common chemical catalysts, they have many advantages, and can catalyze reactions with remarkable catalytic activity and specificity under mild conditions. However, natural enzymes are proteins, RNAs and their complexes which are difficult to acquire, easily denatured and deactivated under various physical or chemical factors, and for these reasons most of them are extraordinarily expensive. Therefore, an understanding of the underlying catalytic principles, structure–function relationships and how to design and synthesize artificial enzymes that are easily prepared, stable, cheap and exhibit similar or higher catalytic activities than natural enzymes based on these principles are of great interest for many scientists.

In the past several decades, considerable efforts have been made to employ various strategies to mimic natural enzymes, such as organic synthesis,[1–4] semi-synthesis,[5] molecular imprinting,[6,7] genetic engineering and so on.[8,9]

State Key Laboratory of Supramolecular Structure and Materials, College of Chemistry, Jilin University, Changchun 130012, People's Republic of China. E-mail: junqiuliu@jlu.edu.cn; luoquan@jlu.edu.cn; Fax: +86-431-85193421

Although the strategies mentioned above are effective to simulate enzymes with extremely high activity and other excellent properties, they are unable to achieve the reasonable match among the catalytic factors of enzymes due to the lack of dynamic ordered structures caused by their stable covalent interactions. To address this problem, a new strategy of supramolecular self-assembly for enzymatic mimicking has been developed recently. The advantages of this strategy are that it is simple, low-cost, dynamic and efficiently generates highly ordered structures with complex architectures to construct tunable artificial enzymes.[10] Since the driving forces of self-assembly are non-covalent interactions like hydrogen bonds, electrostatic interactions, hydrophobic interactions, π–π stacking and so on, enzyme mimics constructed based on this strategy provide several features analogous to natural enzymes: (i) dynamic supramolecular structures; (ii) amphiphilicity of supramolecular architectures; (iii) supramolecular interactions as driving forces for substrate recognition; (iv) specific and/or hydrophobic microenvironments for catalysis.[11] Therefore, the self-assembly strategy is expected to be an alternative way for simulating the structures and functions, and investigating the structure–function relationships and the catalytic mechanisms of natural enzymes.

Among various self-assembled systems, the self-assembly of peptide-based molecules into well ordered nanostructures[12–27]

Published on 05 March 2013 on http://pubs.rsc.org | doi:10.1039/C3TB20156B
Downloaded by University of Tennessee at Knoxville on 18/04/2013 18:10:06.

has aroused great interest for biochemists. Since bioactive peptides are easily synthesized, engineered, chemically modified and biologically functionalized, they are often chosen as suitable building blocks to fabricate nanostructured materials that have many biotechnological applications.[28–34] Reches and Gazit first reported that diphenylalanine dipeptides can self-assemble into nanotubes in water which can be used to produce discrete silver nanowires.[35] Subsequently, Li's group observed that the nanotubes formed from cationic diphenylalanine dipeptide can be transformed into vesicles upon dilution which were used to deliver oligonucleotide into cells.[24] Lately, Stupp and Guler reported a nanofiber hydrolytic catalyst[36] with highly ordered interior constructed from peptide amphiphiles (PAs) which exhibits considerable enhancement in catalytic rate. Up to now a few cases have been reported to use amphiphilic peptide amphiphiles for fabricating artificial enzymes; however, nanotube hydrolase models formed by co-assembly of amphiphilic short peptides have not been reported yet.

Given the fact that the imidazolyl group of histidine plays an important role in the catalytic process of native hydrolase (*e.g.*: chymotrypsin,[37] trypsin,[38] acetylcholine esterase,[39] and kidney dialkylfluorophosphatase[40]), herein we designed and synthesized an imidazolyl-containing amphiphilic tripeptide *N*-(fluorenyl-9-methoxycarbonyl)-Phe-Phe-His-NH_2 (Fmoc-FFH-$CONH_2$) hoping to exploit it to construct a novel supramolecular peptide hydrolase model with high catalytic activity, good biocompatibility and based on it to study the relationships between the ordered arrangement of the supramolecular structures and the catalytic activity. We use peptides as scaffolds because the flexible structures of peptides do make it possible to put the special functional residues of complex proteins into simple molecules, which could further self-assemble into supramolecular structures with abundant orderly arranged functional groups that have many unexpected properties. Moreover, such peptide-assembled structures are also considered low-toxic and biocompatible, and are expected to be applied in organisms as substitutes for natural hydrolases because all constituent units of peptides are derived from natural amino acids. As expected, the synthetic tripeptide can self-assemble into uniform ultra-thin nanotubes with high catalytic activity for *p*-nitrophenyl acetate (PNPA) hydrolysis. In order to investigate if the incorporation of binding sites for substrate PNPA could contribute to the improvement in catalytic activity, different proportions of guanidyl groups in Fmoc-FFR-$CONH_2$ were incorporated into the nanotubes as stable transition state binding sites *via* the co-assembly method. Optimizing the artificial hydrolase enzyme models was achieved through changing the molar ratio of catalytic centers (Fmoc-FFH-$CONH_2$) and binding sites (Fmoc-FFR-$CONH_2$). Then a co-assembled hydrolase model (PepNTs-His-Arg_{max}) that is more efficient than PepNTs-His was obtained. Subsequently, in this report, atomic force microscopic (AFM) imaging was exploited to discuss the relationships between the ordered structure and catalytic activity in detail and an MTT assay was performed to test the cytotoxicity of this peptide-based artificial enzyme.

Materials and methods

Materials

Fmoc-protected amino acids (Fmoc-Phe-OH, Fomc-His(Trt)-OH and Fmoc-Arg(Pbf)-OH), anhydrous *N*-hydroxybenzotriazole (HOBt anhydrous), *N*-methylmorpholine (NMM), benzotriazol-1-yl-oxytripyrrolidinophosphonium hexafluorophosphate (PyBOP) and Rink amide-AM resin were purchased from GL Biochem (Shanghai) Ltd. and used as received. *p*-Nitrophenyl acetate (PNPA) was purchased from J&K Chemical Ltd. (Beijing, China). Other reagents and solvents were purchased from Sigma and used as supplied. Dichloromethane (DCM) and dimethyl formamide (DMF) were purchased commercially, redistilled and subsequently dried with molecular sieves prior to use. All water used was from a Millipore water purification system with a minimum resistivity of 18.0 MΩ cm.

Synthesis and purification of Fmoc-FFH-$CONH_2$ (Scheme 1)

The synthesis and purification of *N*-terminally Fmoc-protected peptides, Fmoc-FFH-$CONH_2$ and Fmoc-FFR-$CONH_2$, were performed using a similar method to that reported previously.[28] Normally, Fmoc-FFH-$CONH_2$ (Fmoc-Phe-Phe-His-$CONH_2$) was constructed on a preloaded Rink amide-AM resin using standard Fmoc (9-fluorenylmethoxycarbonyl) solid peptide phase synthesis techniques on a 0.5 mmol scale. All amide-coupling reactions of peptide synthesis were accomplished for 1.5 hours using 4 equiv. of each amino acid, 4 equiv. of PyBOP, 4 equiv. of HOBt, and 4 equiv. of NMM in DMF. Fmoc removals were carried out with 30 min treatments of 20% (by volume) piperidine–DMF solution. Cleavage of the peptides from the resin was performed with a mixture of trifluoroacetic acid (TFA)–H_2O–triisopropylsilane (95 : 2.5 : 2.5 by volume) for 3 h. The crude peptide product was precipitated and then washed with cold diethyl ether at least four times. The resulting white product was cryo-dried and purified by reversed-phased HPLC on a preparative Varian Dynamax C18 column under linear elution gradients of CH_3CN–water (30/70, 0.1% TFA) over 30 minutes. Peptide purity was assessed by analytical reversed-phase HPLC (>98%) and characterized using a Bruker 300 MHz spectrometer and matrix assisted laser desorption ionization-time of flight mass spectrometer (MALDI-TOF MS).

^{1}H NMR (300 MHz, DMSO-d_6, 25 °C) δ (ppm): 8.85 (s, 1H), 8.34 (d, 1H), 8.26 (d, 1H), 7.88 (d, 2H), 7.59 (t, 2H), 7.53 (d, 1H), 7.40 (t, 3H), 7.24 (m, 15H), 4.49 (s, 2H), 4.06–4.27 (m, 5H), 2.53–3.13 (m, 5H). $C_{39}H_{38}N_6O_5$ *m*/*z* (ES) 693.2 $[M + Na]^+$.

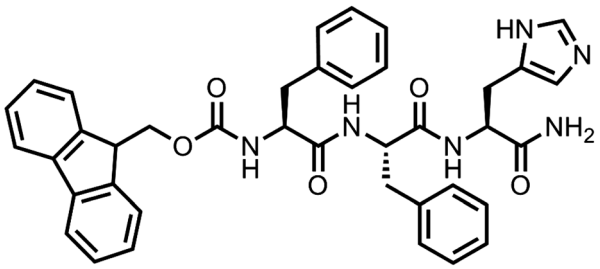

Scheme 1 The structure of Fmoc-FFH-$CONH_2$.

This journal is © The Royal Society of Chemistry 2013

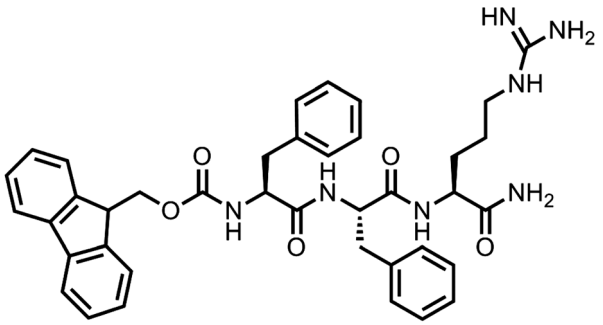

Scheme 2 The structure of Fmoc-FFR-$CONH_2$.

Downloaded by University of Tennessee at Knoxville on 18/04/2013 18:10:06.
Published on 05 March 2013 on http://pubs.rsc.org | doi:10.1039/C3TB20156B

Synthesis and purification of Fmoc-FFR-$CONH_2$ (Scheme 2)

The synthesis and purification of Fmoc-FFR-$CONH_2$ were similar to those of Fmoc-FFH-$CONH_2$ with the same amide-coupling, Fmoc removal and purification steps except that cleavage of the peptides from the resin was performed with a mixture of trifluoroacetic acid (TFA)–thioanisole–H_2O–phenol–1,2-ethanedithiol (EDT)–triisopropylsilane (81.5 : 5 : 5 : 5 : 2.5 : 1 by volume). The purified peptide was characterized using a Bruker 300 MHz spectrometer and matrix assisted laser desorption ionization-time of flight mass spectrometer (MALDI-TOF MS).

^{1}H NMR (300 MHz, DMSO-d_6, 25 °C) δ (ppm): 8.14 (2H, m), 7.89 (2H, d), 7.60 (3H, m), 7.48 (1H, t), 7.40 (3H, m), 7.22 (15H, m), 4.57 (1H, m), 4.20 (2H, m), 4.10 (2H, m), 3.08 (3H, m), 2.89 (2H, d), 2.72 (1H, m), 1.68 (1H, m), 1.48 (3H, m). $C_{39}H_{43}N_7O_5$ *m/z* (ES) 712.4 $[M + Na]^+$.

Preparation of self-assembled peptide nanotube hydrolase model PepNTs-His

Fmoc-FFH-$CONH_2$ was dissolved in dimethyl sulfoxide (DMSO) at a concentration of 50 mM. The self-assembled peptide nanotubes (PepNTs-His) were prepared by diluting the stock solution with ultra-pure water to a final peptide concentration of 1 mM with pH = 7.5.

Preparation of co-assembled peptide nanotube hydrolase models PepNTs-His-Args

Different proportions of Fmoc-FFH-$CONH_2$ and Fmoc-FFR-$CONH_2$ were mixed in dimethyl sulfoxide (DMSO) with a fixed concentration of 50 mM of Fmoc-FFH-$CONH_2$. The co-assembled peptide nanotubes (PepNTs-His-Arg) were prepared by diluting the stock solution with ultra-pure water to a final Fmoc-FFH-$CONH_2$ concentration of 1 mM with pH = 7.5.

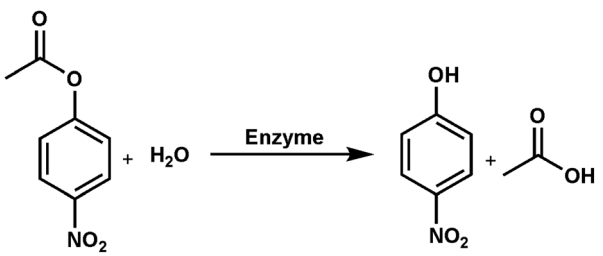

Fig. 1 The hydrolysis process of PNPA in the presence of enzyme.

Characterization of the co-assembly behaviour

Fmoc-FFH-$CONH_2$ and Fmoc-FFR-$CONH_2$ at a molar ratio of 1 : 1 were mixed in deuterated DMSO (DMSO-d_6) at a total concentration of 100 mM. The stock solution was then diluted with deuteroxide to a final concentration of 2 mM. Individual 1 mM Fmoc-FFH-$CONH_2$ and Fmoc-FFR-$CONH_2$ aqueous solutions were also prepared as controls. The fresh samples were characterized by ^{1}H NMR spectroscopy. Changes of peaks on Fmoc groups, benzene rings and imidazolyls before and after co-assembly were compared to identify if these two molecules could co-assemble.

Determination of the catalytic activity for PNPA hydrolysis

The catalytic activity was monitored using PNPA as substrate (see Fig. 1). The reaction was carried out at 25 °C in 500 μL of *N*-(2-hydroxyethyl)piperazine-*N*′-ethanesulfonic acid (HEPES) buffer (pH = 7.5, 10 mM) containing 0.1 mM of peptide nanotube catalyst and 0.5 mM of PNPA. Considering the UV spectrum of the hydrolytic product 4-nitrophenol which exhibits a strong absorption peak at 400 nm, the initial reaction rates were determined by monitoring the absorption increase at 400 nm with a Shimadzu 2450 UV-VIS-NIR spectrophotometer. The appropriate control activity without peptide nanotube catalyst was also assayed and subtracted from the catalyzed reaction. The detailed process occurred as follows: first, in a 0.5 mL quartz cuvette, 400 μL of HEPES buffer (pH 7.5, 10 mM) and 50 μL of the peptide nanotube catalyst (1 mM) were added and thermally equilibrated for 2 min. The reaction was initiated by addition of 50 μL substrate PNPA solution (0.5 mM). The absorption increase at λ = 400 nm due to the release of product 4-nitrophenol was recorded.

Cell culture

HeLa cells (epithelial cervical cancer cell line) in Dulbecco's modified Eagle medium (Invitrogen, Carlsbad, CA) were added to each well of a 96-well plate supplemented with 10% fetal bovine serum (FBS), 100 U mL^{-1} penicillin, and 100 mg mL^{-1} streptomycin. The cells were grown in a humidified incubator (37 °C, 5% CO_2) and seeded at a density of 1×10^5 cells per well. After incubation for 12 h, the cells of ~80% confluence were further incubated with fresh medium containing PepNTs-His or PepNTs-His-Arg_{max} with set concentrations (from 1 to 100 μM) for another 24 h. Then 10 mL of 5 mg mL^{-1} thiazolyl blue tetrazolium bromide (MTT, Sigma-Aldrich, USA) solution was added. After incubation at 37 °C for 4 h. DMSO (Sigma, USA) solution was added to each well to lyse the cells. The absorbance of supernatants was measured at 570 nm by using a microplate reader (Bio-Rad ELX800, USA).

Instruments and measurement

Atomic force microscopy (AFM), transmission electron microscopy (TEM), circular dichroism (CD), Fourier transform infrared

Downloaded by University of Tennessee at Knoxville on 18/04/2013 18:10:06.
Published on 05 March 2013 on http://pubs.rsc.org | doi:10.1039/C3TB20156B

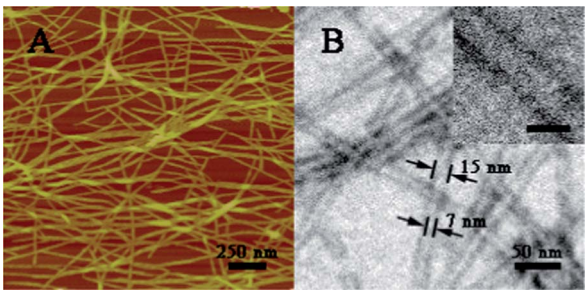

Fig. 2 (A) Height AFM image of nanotubes self-assembled from Fmoc-FFH-$CONH_2$ (PepNTs-His) in aqueous solution at concentration of 1 mM. (B) TEM micrograph and HR-TEM micrograph (inset, scale bar is 10 nm) of PepNTs-His, which was stained with 2% phosphotungstic acid before imaging.

(FTIR) spectroscopy, fluorescence emission spectroscopy and UV-vis spectroscopy measurements were performed to characterize the structural conformations and morphologies of PepNTs-His and PepNTs-His-Arg. The CD spectra were collected on a Jasco J-810 spectropolarimeter under a nitrogen atmosphere. AFM imaging was performed on a NanoScope Multi-Mode-AFM (Veeco, USA). TEM measurements were performed on a JEOL model JEM-3010 at 300 kV. All samples were stained with 2% phosphotungstic acid. FT-IR spectra were obtained on a Bruker Vector 22 FT-IR spectrometer at ambient temperature. UV-vis spectra were measured on a Shimadzu 3100 UV-vis-NIR spectrophotometer. Fluorescence emission spectra were recorded on a Perkin-Elmer LS-55 luminance spectrometer. ^{1}H NMR spectra were obtained using a Bruker AVANCE III 500 apparatus.

Results

Characterization of the self-assembled nanotubes

AFM images (Fig. 2A) clearly show the formation of uniform, high aspect ratio cylindrical nanostructures with diameters about 10 nm and length of several micrometers. The dense nanotubes were intertwined into a net structure, which was further supported by the hydrogelation of Fmoc-FFH-$CONH_2$ at a higher concentration. Transmission electron microscopy (TEM) has also been performed to investigate the morphology of the peptide nanotubes. TEM images after negative staining (Fig. 2B) also obviously revealed the generation of cylindrical nanotubes with dark walls and relatively off-white hollows. These nanotubes have external diameters between 14 and 16 nm, inner diameters between 6 and 8 nm and lengths up to several micrometers. This is consistent with the AFM results. Dynamic light scattering (DLS) was further utilized to study the aggregation behavior of the Fmoc-peptides in aqueous solution. The results (>100 nm) reveal that the Fmoc-peptides can form a nano-scale structure in aqueous solution through self-assembly into uniform nanotubes.

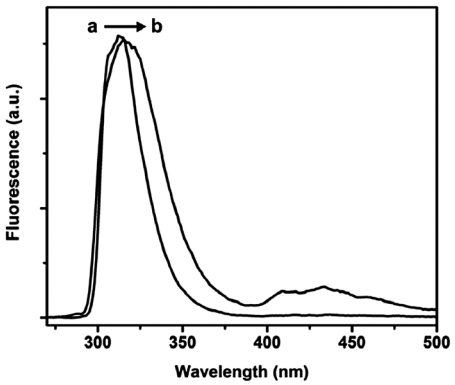

Fig. 4 Fluorescence emission spectra of Fmoc-FFH-$CONH_2$ peptide nanotubes (PepNTs-His) at concentrations of 0.01 mM (a) and 0.1 mM (b).

Characterization of the secondary structure of the peptide nanotubes

Circular dichroism (CD) and Fourier-transform infrared (FT-IR) spectroscopy were employed to study the backbone orientation of Fmoc-FFH-$CONH_2$ in the nanotubes. A negative peak at 218 nm in the CD spectrum was detected, indicating the presence of β-sheet structures in the molecular assembly (Fig. 3A).[30] This assertion was further supported by FT-IR spectroscopy study (Fig. 3B). The FT-IR spectrum of Fmoc-FFH-$CONH_2$ nanotubes exhibited absorption peaks at around 1640 and 1690 cm^{-1}, which are consistent with a β-sheet structure and an anti-parallel arrangement of the peptides.[30,41]

In order to comprehensively investigate the self-assembly mechanism, fluorescence emission spectroscopy was employed to explore the internal microenvironment among the fluorenyl (Fmoc) moieties of Fmoc-FFH-$CONH_2$ (Fig. 4). At a low

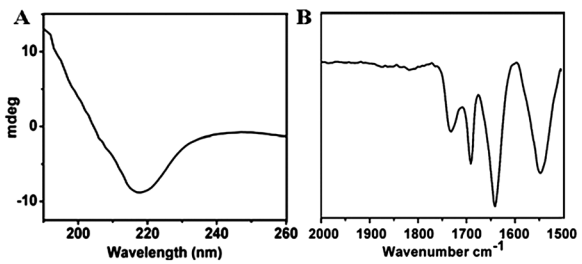

Fig. 3 (A) Circular dichroism spectrum and (B) FT-IR spectrum of Fmoc-FFH-$CONH_2$ peptide nanotubes (PepNTs-His) at a concentration of 0.1 mM.

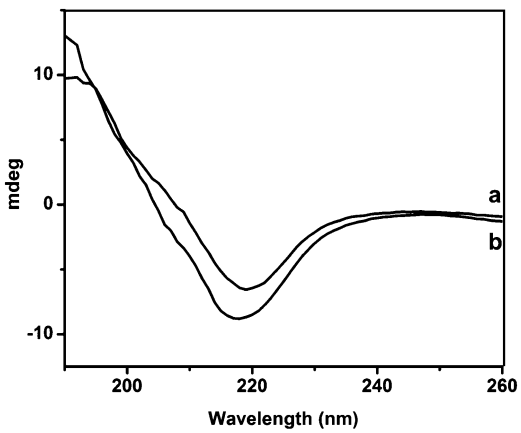

Fig. 5 Circular dichroism spectra of PepNTs-His (a) and PepNTs-His-Arg_{max} (b).

This journal is © The Royal Society of Chemistry 2013

Downloaded by University of Tennessee at Knoxville on 18/04/2013 18:10:06.
Published on 05 March 2013 on http://pubs.rsc.org | doi:10.1039/C3TB20156B

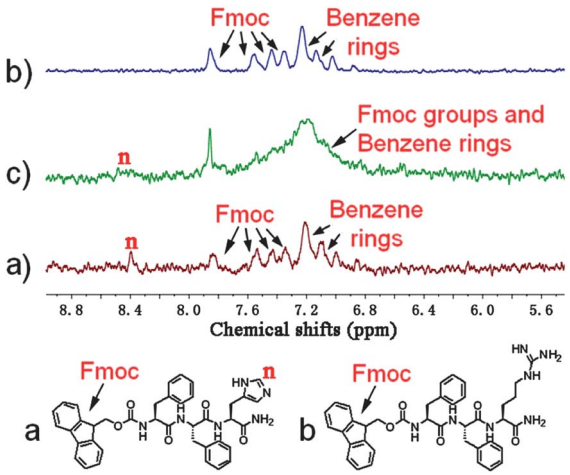

Fig. 6 ^{1}H NMR spectra of Fmoc-FFH-$CONH_2$ (a), Fmoc-FFR-$CONH_2$ (b) and their mixture (c) in D_2O.

concentration of 0.01 mM, PepNTs-His exhibits a sharp emission peak at 311 nm. As the concentration increases to 0.1 mM, the emission peak shifts to 318 nm. The red-shift is caused by the interaction of the Fmoc groups of Fmoc-FFH-$CONH_2$ during the self-assembly process,[42,43] which also indicates an anti-parallel arrangement of fluorenyl rings.[30] A broad feature with a maximum at 432 nm in the emission spectrum of Fmoc-FFH-$CONH_2$ was detected, implying an extensive J-aggregate of phenyl rings as well as fluorenyl rings.[30] Similar aggregates were reported previously in other systems.[44] The analytical results from fluorescence spectra indicate that π–π stacking interactions assisted by hydrogen bonds can act as important driving forces in Fmoc-peptide assembly and the Fmoc-peptide assembly predominantly aggregates in an anti-parallel β-sheet manner.

CD measurement was employed to investigate whether the addition of small amounts of Fmoc-FFR-$CONH_2$ to Fmoc-FFH-$CONH_2$ would change the secondary structure of the peptide nanotubes. The comparison of the CD spectra of PepNTs-His and PepNTs-His-Arg showed that both types of nanotubes exhibit extremely similar negative peaks at 218 nm (Fig. 5), which means that the incorporation of small amounts of Fmoc-FFR-$CONH_2$ into Fmoc-FFH-$CONH_2$ nanotubes does not interrupt the inner secondary structure. Namely, these two types of nanotubes have the same β-sheet arrangement and aggregate behavior.

Characterization of the co-assembly of PepNTs-His-Arg

^{1}H NMR spectroscopy was performed in D_2O solutions made up of Fmoc-FFH-$CONH_2$, Fmoc-FFR-$CONH_2$ and their mixture to investigate the co-assembly of these two molecules. Representative relatively sharp peaks of Fmoc groups and benzene rings were observed in both cases of individual Fmoc-FFH-$CONH_2$ (Fig. 6a) and Fmoc-FFR-$CONH_2$ (Fig. 6b). When they were mixed, the sharp peaks disappear and a broad peak appears (Fig. 6c). What's more, after mixing, the original obvious peaks (Fig. 6a) on the imidazolyls of Fmoc-FFH-$CONH_2$ were shifted

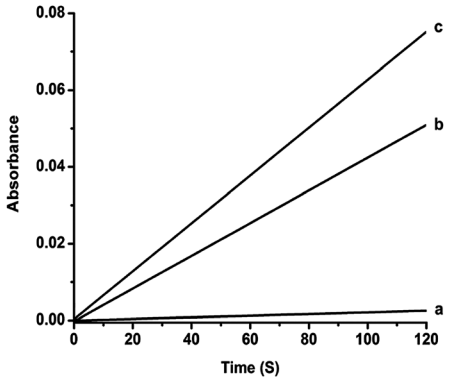

Fig. 7 Plots of absorbance *vs.* time for hydrolysis of PNPA (0.5 mM). (a) Control, (b) PepNTs-His, (c) PepNTs-His-Arg_{max}.

and cleaved (Fig. 6c). The fact that the observed broad peak of the mixture is not merely a superposition of individual peaks of the two components strongly supports the formation of the mixed nanotubes in which two molecules form a single aggregate structure (PepNTs-His-Arg). The broad peak of Fmoc groups and benzene rings also reveals that the Fmoc groups and benzene rings interacted with each other which further confirms the assertion mentioned above that an extensive J-aggregate of phenyl rings as well as fluorenyl rings exists in the nanotubes.

Catalytic behaviour

The initial hydrolytic rate was measured according to the increased absorption value of the hydrolytic product *p*-nitrophenol at 400 nm. The hydrolytic rate against PNPA without enyzme is very slow (Fig. 7a). The addition of PepNTs-His results in a distinct enhancement (Fig. 7b). When Fmoc-FFR-$CONH_2$ was incorporated into the PepNTs-His nanotubes as the binding site of the stable transition state, under identical conditions, a higher hydrolytic rate was observed (Fig. 7c) which means the co-assembled peptide nanotube hydrolase model is more effective than the self-assembled one. This results implies that the catalytic activity of enzyme models can be improved by appropriately strengthening the binding of the stable transition state.

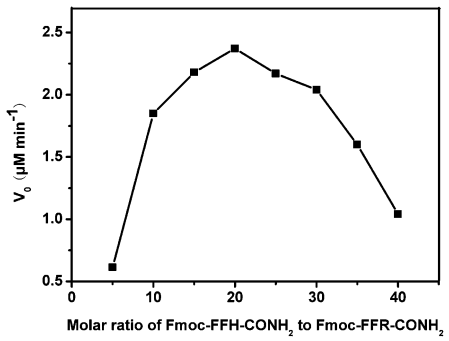

Fig. 8 Plots of catalytic reaction rates for hydrolysis of PNPA (0.5 mM) *vs.* molar ratio of Fmoc-FFH-$CONH_2$ to Fmoc-FFR-$CONH_2$. The concentration of Fmoc-FFH-$CONH_2$ was fixed at 0.1 mM.

Downloaded by University of Tennessee at Knoxville on 18/04/2013 18:10:06.
Published on 05 March 2013 on http://pubs.rsc.org | doi:10.1039/C3TB20156B

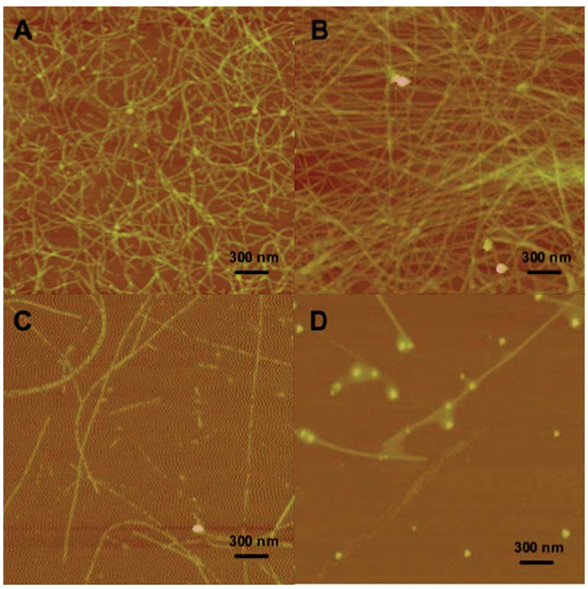

Fig. 9 Height AFM images of nanotubes induced by the molar ratio of Fmoc-FFH-$CONH_2$ to Fmoc-FFR-$CONH_2$: (A) 40 : 1; (B) 20 : 1; (C) 10 : 1; (D) 2 : 1.

Optimization of the co-assembled hydrolase model

To determine whether the incorporation of Fmoc-FFR-$CONH_2$ can achieve higher catalytic activity, a series of co-assembled peptide nanotubes were prepared by optimizing the molar ratio between Fmoc-FFH-$CONH_2$ and Fmoc-FFR-$CONH_2$. In this experimental process, the concentration of Fmoc-FFH-$CONH_2$ was kept constant at 1 mM while the concentration of Fmoc-FFR-$CONH_2$ was varied. The catalytic activities of different co-assembled nanotube models were measured under the same conditions. As shown in Fig. 8, the initial hydrolytic rates of co-assembled nanotube models can be divided into two stages according to the increase of molar ratio of these two building blocks (Fmoc-FFH-$CONH_2$–Fmoc-FFR-$CONH_2$). From 40 : 1 to 20 : 1, the initial rate increases with the increase of Fmoc-FFR-$CONH_2$. Then the initial hydrolytic rate decreases even though the molar ratio keeps increasing from 20 : 1 to 2 : 1, revealing that the initial hydrolytic rate is optimal at the molar ratio of 20 : 1.

AFM images were used to explore the details that cause this interesting phenomenon. As shown in Fig. 9, from 40 : 1 to 20 : 1, just a small amount of Fmoc-FFR-$CONH_2$ was incorporated into the nanotubes, and there was no obvious structural change observed. The co-assembled peptide nanotubes have similar shapes as the self-assembled peptide nanotubes. However, as the molar ratio of Fmoc-FFH-$CONH_2$–Fmoc-FFR-$CONH_2$ decreased below 20 : 1, the nanotube structures were gradually damaged. It is suggested that the well ordered supramolecular structure of the peptide nanotubes plays an important role in their catalytic activity. A similar phenomenon had also been described by Stupp and Guler.[36] At high proportion of Fmoc-FFH-$CONH_2$ to Fmoc-FFR-$CONH_2$, the greater the amount of Fmoc-FFR-$CONH_2$, the higher the catalytic activity. This is mainly due to the transition state being gradually stabilized with the increase of Fmoc-FFR-$CONH_2$. However, once the proportion of Fmoc-FFH-$CONH_2$ to Fmoc-FFR-$CONH_2$ is below 20 : 1, then the catalytic activity decreases. This is mainly due to the damaged nanotube scaffolds influencing the reasonable distribution of the catalytic centers and binding sites. On the other hand, when the amount of Fmoc-FFR-$CONH_2$ is large enough and the substrate-binding ability endowed from Fmoc-FFR-$CONH_2$ increases to a higher degree, the excessively strongly binding of substrates will prevent the products from moving away from the catalytic centers, thus making the completion of the catalytic cycle inefficient,[45–47] and resulting in lower catalytic activity. At a molar ratio of 20 : 1, the nanotube structure remains stable and the catalytic centers and binding sites match each other well, leading to the maximum catalytic activity and the optimal peptide nanotube hydrolase model.

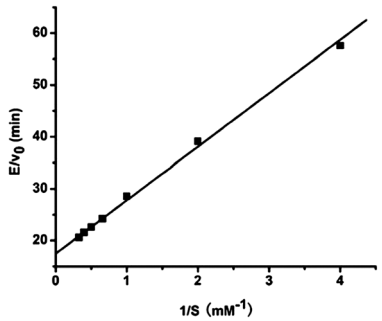

Fig. 10 Lineweaver–Burk plots for the hydrolysis of PNPA catalyzed by PepNTs-His-Arg_{max} (0.1 mM catalytic center Fmoc-FFH-$CONH_2$, Fmoc-FFH-$CONH_2$: Fomc-FFR-$CONH_2$ = 20 : 1).

Enzymatic behaviour

Hydrolytic reaction was carried out at all individual concentrations of PNPA to investigate the enzymatic properties of the co-assembled nanotube model (Fig. 10). A typical enzymatic saturation kinetics (Fig. 11) was measured which proved it to be a real enzyme model for ester hydrolysis. The apparent kinetic parameters were calculated based on the Michaelis–Menten equation: $k_{cat(app)} = 1.38 \times 10^{-3}\ s^{-1}$, $K_m = 0.76$ mM, $k_{cat(app)}$/

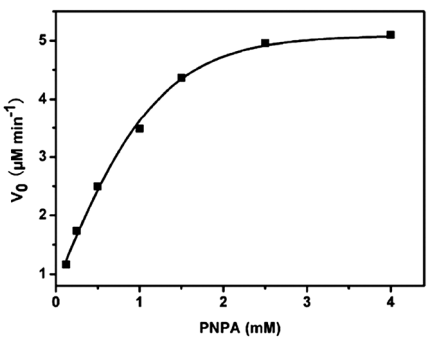

Fig. 11 Plot of initial catalytic reaction rate *vs.* concentration of PNPA in the presence of PepNTs-His-Arg_{max} (0.1 mM catalytic center Fmoc-FFH-$CONH_2$, Fmoc-FFH-$CONH_2$: Fomc-FFR-$CONH_2$ = 20 : 1).

This journal is © The Royal Society of Chemistry 2013

Downloaded by University of Tennessee at Knoxville on 18/04/2013 18:10:06.
Published on 05 March 2013 on http://pubs.rsc.org | doi:10.1039/C3TB20156B

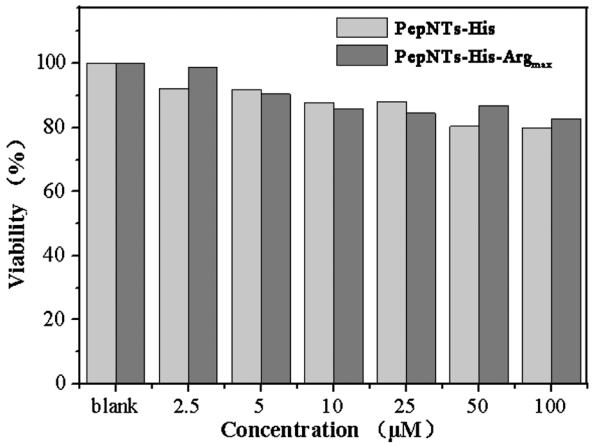

Fig. 12 Cytotoxicity of PepNTs-His and PepNTs-His-Arg$_{max}$ at different concentrations. The viability of HeLa cells incubated with different concentrations (μM) of PepNTs-His for 24 h.

$K_m = 1.82\ M^{-1}\ s^{-1}$, $k_{cat(app)}/k_{uncat} = 519$. This means a single catalytic center of the nanotubes exhibits 519-fold higher catalytic activity for PNPA hydrolysis compared to that without catalyst. Given a nanotube with multi-catalytic centers, supramolecular nanoenzymes would exhibit more remarkable catalytic activity.

Cytotoxicity study of PepNTs-His and PepNTs-His-Arg$_{max}$

An MTT assay was performed to evaluate the cytotoxicity of PepNTs-His and PepNTs-His-Arg$_{max}$. The effect of the nanotubes on the proliferation of HeLa was studied (Fig. 12). After 24 h of incubation, a slight decrease in cell viability was observed. Even increasing the concentration of the peptide nanotubes to 100 μM (67 μg mL^{-1}), it displayed only a mild decrease in human cell viability, which obviously suggested that the peptide-based nanotubes have reasonably good biocompatibility with human cells.

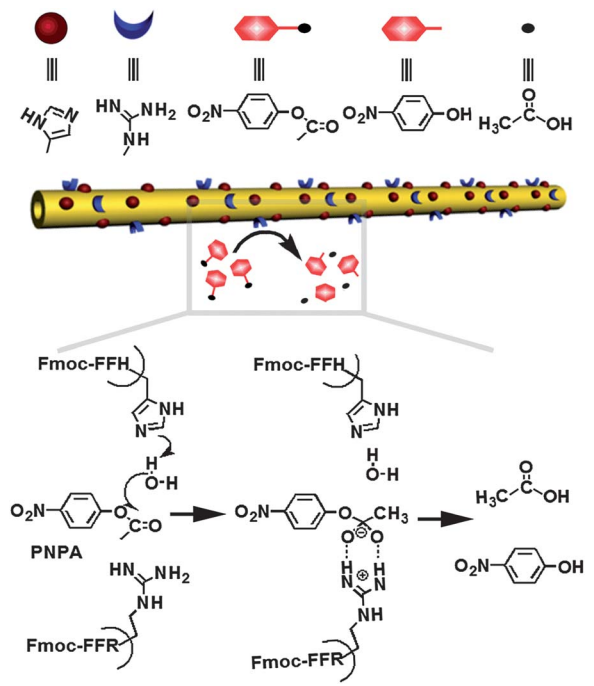

Scheme 3 Schematic representation of the possible mechanism for the cleavage of PNPA catalyzed by PepNTs-His-Arg$_{max}$.

Proposed catalytic mechanism

Scheme 3 graphically describes the possible catalytic mechanism of the co-assembled peptide nanotube hydrolase model. First, the hydrophobic interior of the peptide nanotubes can help to bind the benzene ring of aromatic substrate PNPA. Second, an imidazolyl of histidine residue binds a proton of H_2O molecule to activate the hydroxide ion. The hydroxide ion, as a nucleophilic moiety, further attacks the carbonyl of PNPA to generate a tetrahedral transition state. Finally, a guanidyl on the co-assembled nanotubes binds the oxide ions of the tetrahedral intermediate complex to stabilize the tetrahedral transition state and activates the C–O bond for its cleavage. Product *p*-nitrophenol is then released and the next catalysis cycle begins.

Conclusions

In conclusion, a novel nanotube hydrolase model self-assembled from synthetic amphiphilic short peptide Fmoc-FFH-$CONH_2$ has been prepared. Taking advantage of the hydrophobic microenvironment provided by the Fmoc-FF aromatic ring segments and the catalytic center histidines loaded on the self-assembled peptide nanotubes, this model exhibits higher catalytic activity for PNPA hydrolysis compared to that without catalyst. Then Fmoc-FFR-$CONH_2$ which contains guanidyls, the binding groups for carbonyls, was incorporated into the Fmoc-FFH-$CONH_2$ nanotubes to form a co-assembled peptide nanotube hydrolase model. At a suitable molar ratio of Fmoc-FFH-$CONH_2$–Fmoc-FFR-$CONH_2$, the co-assembled model exhibits the highest catalytic ability. A comparison of the catalytic activity between PepNTs-His and PepNTs-His-Arg combined with the AFM results reveals that both a well-ordered dynamic supramolecular structures and the reasonable match between the catalytic centers and binding sites play important roles in the improvement of the catalytic activity of artificial enzymes. More importantly, this novel peptide hydrolase model is biocompatible with human cells which is promising for use as substitutes for natural hydrolases to treat inflammation, anorexia, edema and other diseases.

Acknowledgements

We are grateful for the financial support from the Natural Science Foundation of China (no: 21234004, 91027023, 21221063, 21004028), Changchun Institute of Applied Chemistry (RERU2011008) and the Ministry of Education of China.

Notes and references

1 J. A. Gerlt and P. C. Babbitt, *Curr. Opin. Chem. Biol.*, 2009, **13**, 10–18.
2 Z. Y. Dong, J. Q. Liu, S. Z. Mao, X. Huang, B. Yang, G. M. Luo and J. C. Shen, *J. Am. Chem. Soc.*, 2004, **126**, 16395–16404.

Downloaded by University of Tennessee at Knoxville on 18/04/2013 18:10:06.
Published on 05 March 2013 on http://pubs.rsc.org | doi:10.1039/C3TB20156B

3 R. Breslow and B. Zhang, *J. Am. Chem. Soc.*, 1992, **114**, 5882–5883.
4 R. Breslow and B. Zhang, *J. Am. Chem. Soc.*, 1994, **116**, 7893–7894.
5 Z. P. Wu and D. Hilvert, *J. Am. Chem. Soc.*, 1989, **111**, 4513–4514.
6 W. B. Motherwell, C. E. Atkinson, A. E. Aliev, S. Y. F. Wong and B. H. Warrington, *Angew. Chem., Int. Ed.*, 2004, **43**, 1225–1228.
7 J. Q. Liu and G. Wulff, *J. Am. Chem. Soc.*, 2008, **130**, 8044–8054.
8 A. J. Kirby, *Angew. Chem., Int. Ed. Engl.*, 1996, **35**, 707–724.
9 X. M. Liu, L. A. Silks, C. P. Liu, M. Ollivault-Shiflett, X. Huang, J. Li, G. M. Luo, Y. M. Hou, J. Q. Liu and J. C. Shen, *Angew. Chem., Int. Ed.*, 2009, **48**, 2020–2023.
10 X. Huang, X. M. Liu, Q. Luo, J. Q. Liu and J. C. Shen, *Chem. Soc. Rev.*, 2011, **40**, 1171–1184.
11 Z. Y. Dong, Y. G. Wang, Y. Z. Yin and J. Q. Liu, *Curr. Opin. Colloid Interface Sci.*, 2011, **16**, 451–458.
12 W. Hamley, *Angew. Chem., Int. Ed.*, 2007, **46**, 8128–8147.
13 M. Vestergaard, T. Hamada and M. Takagi, *Biotechnol. Bioeng.*, 2008, **99**, 753–763.
14 X. Zhao and S. Zhang, *Trends Biotechnol.*, 2004, **22**, 470–476.
15 E. Gazit, *Chem. Soc. Rev.*, 2007, **36**, 1263–1269.
16 X. Zhao and S. Zhang, *J. Mater. Chem.*, 2004, **14**, 2082–2086.
17 Y. Jin, X. Xu, C. Chen, S. Cheng, X. Zhang and R. Zhuo, *Macromol. Rapid Commun.*, 2008, **29**, 1726–1730.
18 R. V. Ulijn and A. M. Smith, *Chem. Soc. Rev.*, 2008, **37**, 664–675.
19 W. Hamley, *Soft Matter*, 2011, **7**, 4122–4138.
20 M. Reches and E. Gazit, *Science*, 2003, **300**, 625–627.
21 Z. A. C. Schnepp, R. Gonzalez-McQuire and S. Mann, *Adv. Mater.*, 2006, **18**, 1869–1872.
22 M. Smith, R. J. Williams, C. Tang, P. Coppo, R. F. Collins, M. L. Turner, A. Saiani and R. V. Ulijn, *Adv. Mater.*, 2008, **20**, 37–41.
23 R. Orbach, L. Adler-Abramovich, S. Zigerson, I. Mironi-Harpaz, D. Seliktar and E. Gazit, *Biomacromolecules*, 2009, **10**, 2646–2651.
24 X. Yan, Q. He, K. Wang, L. Duan, Y. Cui and J. Li, *Angew. Chem., Int. Ed.*, 2007, **46**, 2431–2434.
25 X. Yan, P. Zhu and J. Li, *Chem. Soc. Rev.*, 2010, **39**, 1877–1890.
26 J. Ryu and C. B. Park, *Adv. Mater.*, 2008, **20**, 3754–3758.
27 S. Toledano, R. J. Williams, V. Jayawarna and R. V. Ulijn, *J. Am. Chem. Soc.*, 2006, **128**, 1070–1071.
28 Y. G. Wang, L. N. Cao, S. W. Guan, G. N. Shi, Q. Luo, L. Miao, I. Thistlethwaite, Z. P. Huang, J. Y. Xu and J. Q. Liu, *J. Mater. Chem.*, 2012, **22**, 2575–2581.
29 J. Wang, Z. Wang, J. Gao, L. Wang, Z. Yang, D. Kong and Z. Yang, *J. Mater. Chem.*, 2009, **19**, 7892–7896.
30 R. V. Ulijn, *J. Mater. Chem.*, 2006, **16**, 2217–2225.
31 V. Jayawarna, M. Ali, T. A. Jowitt, A. F. Miller, A. Saiani, J. E. Gough and R. V. Ulijn, *Adv. Mater.*, 2006, **18**, 611–614.
32 X. Xu, L. Liang, C. Chen, B. Lu, N. Wang, F. Jiang, X. Zhang and R. Zhuo, *ACS Appl. Mater. Interfaces*, 2010, **2**, 2663–2671.
33 Z. Yang and B. Xu, *J. Mater. Chem.*, 2007, **17**, 2385–2393.
34 Z. Yang, G. Liang and B. Xu, *Acc. Chem. Res.*, 2008, **41**, 315–326.
35 M. Reches and E. Gazit, *Science*, 2003, **300**, 625–627.
36 M. O. Guler and S. I. Stupp, *J. Am. Chem. Soc.*, 2007, **129**, 12082–12083.
37 H. Gutfreund and J. M. Sturtevant, *Biochem. J.*, 1956, **63**, 656–661.
38 N. M. Godzhaev, *Mol. Biol.*, 1984, **18**, 1432–1435.
39 M. A. Massiah, C. Viragh, P. M. Reddy, I. M. Kovach, J. Johnson, T. L. Rosenberry and A. S. Mildvan, *Biochemistry*, 2001, **40**, 5682–5690.
40 F. Bergmann, R. Segal and S. Rimon, *Biochem. J.*, 1957, **67**, 481–486.
41 A. Barth and C. Zscherp, *Q. Rev. Biophys.*, 2002, **35**, 369–429.
42 O. Carny, D. E. Shalev and E. Gazit, *Nano Lett.*, 2006, **8**, 1594–1597.
43 R. Djalali, Y. Chen and H. Matsui, *J. Am. Chem. Soc.*, 2002, **124**, 13660–13661.
44 B. Song, H. Wei, Z. Q. Wang, X. Zhang, M. Smet and W. Dehaen, *Adv. Mater.*, 2007, **19**, 416–420.
45 Y. Z. Yin, L. Wang, H. Y. Jin, C. Y. Lv, S. J. Yu, X. Huang, Q. Luo, J. Y. Xu and J. Q. Liu, *Soft Matter*, 2011, **7**, 2521–2529.
46 X. Huang, Y. Liu, K. Liang, Y. Tang and J. Q. Liu, *Biomacromolecules*, 2008, **9**, 1467.
47 S. J. Yu, Y. Z. Yin, J. Y. Zhu, X. Huang, Q. Luo, J. Y. Xu, J. C. Shen and J. Q. Liu, *Soft Matter*, 2010, **6**, 5342–5350.

 This journal is © The Royal Society of Chemistry 2013